



Journal of Applied and Computational Mechanics



Research Paper

Calculation of Backscattered Ultrasonic Waves Field from a Copper-clad Steel Rod Immersing in Water and Effect of Clad Corrosion and Interfacial Disbond between Clad and Rod Defects on this Field using the Finite Element Method

Omid Noormohammadi Arani¹, Mehdi Zeighami Salimabad², Amin Yaghootian³,
Mohammadreza Kari⁴

¹ Mechanical Engineering Department, Faculty of Engineering, Shahid Chamran University of Ahvaz,
Golestan Blvd., Ahvaz, 61357-43337, Iran, Email: omidnoormohammadi4@gmail.com

² Medical Physics Dept., SMPH, University of Wisconsin – Madison, USA, Email: zeighamisali@wisc.edu

³ Mechanical Engineering Department, Faculty of Engineering, Shahid Chamran University of Ahvaz,
Golestan Blvd., Ahvaz, 61357-43337, Iran, Email: a.yaghootian@scu.ac.ir

⁴ Medical Physics Dept., SMPH, University of Wisconsin – Madison, USA, Email: mkari@wisc.edu

Received August 07 2021; Revised October 16 2021; Accepted for publication November 04 2021.

Corresponding author: M. Zeighami Salimabad (zeighamisali@wisc.edu)

© 2021 Published by Shahid Chamran University of Ahvaz

Abstract. Inspection and specificity of the intactness of multi-layer and small-size parts like copper-clad steel rod is a hard task and requires high accuracy. The intactness of these parts is crucial due to their importance. One of the inspection methods for these parts is using ultrasonic waves. The scattering phenomenon occurs when these waves impact curved shape bodies under a special condition. The ultrasonic scattering waves contain a lot of information from the physical conditions and mechanical properties of the part. However, using these waves requires high accuracy and attention due to their complexity. One result of the ultrasonic scattering waves is the far-field backscattered frequency spectrum, form function. For the first time in this research, the form function of a copper-clad steel rod that is immersed in water is calculated using the finite element method (FEM) available in the commercial ABAQUS software. For validating the proposed model, the simulation results are compared with analytical and experimental results in the normalized frequency range of $4 \leq Ka \leq 10$. A good agreement is observed between the three methods at the resonance frequencies, and in the overall form of obtained form function. Furthermore, the effects of the two most common defects in these rods, i.e., the corrosion and interfacial disbond between the clad and steel rod, is studied. Results show that this method can properly specify the corrosion percentage and location, and also the length and location of the interfacial disbond defect.

Keywords: Ultrasonic waves; Finite element method; Scattering; Form function; Corrosion; Surface interfacial disbond.

1. Introduction

Increasing the resistance and decreasing the cost are two opposite needs in modern industry. The cladding has considerably solved this problem, such that in addition to a considerable increase in useful properties of the parts, including a decrease in the corrosion tendency, increasing the mechanical resistance and conductance, etc. the production cost of them is also decreased. A quick and common inspection of industrial multi-layered parts with no damages to them has always been under the attention of scientists and researchers. The ultrasonic waves are one of the methods used for inspecting complex structures [1-4]. However, using this method involves special complexities when the part dimensions are small, such as the steel rods with copper-clad. Since the ultrasonic wave field is influenced by the geometrical features and physical properties of the scatterer body, the study of these waves provides the properties inspection and survey of the part under ultrasonic radiation.

One pieces of information obtained from the ultrasonic wave field is the far-field backscattered frequency spectrum, or form function [5]. These diagrams are evaluated using Resonance Acoustic Spectroscopy (RAS). Faran [6] analytically investigated the wave scattering from the isotropic sphere or cylinder immersing in the water. Flex et al. [7] and Garan et al. [8] studied interference of the surface waves around the elastic body, and the formation of standing waves. The mathematical model for calculating the form function of the sonic waves from transverse isotropic cylinders immersed in the fluid was proposed by Honarvar and Sinclair [9] using the normal mode expansion. Ripoché et al. [10] invented the first experimental method based on the method of identification and isolation of resonance. Using the reflection echo of the wave, as the reference frequency spectrum in the method



of identification and isolation of resonance, was proposed by Sodagar et al. [11] using the short pulse waves. Using this reference spectrum, the inconsistency between the scattering signal and reference frequency spectrums in large-diameter rods, which caused a lack of accuracy and decrease in the effective frequency range of the form function, is solved. Jamali et al. [12] studied the scattering equations of a Functionally Graded Materials (FGMs) cylinder using the state-space method and normal mode expansion. Romanov and Tolokonnikov [13] analytically calculated the sonic's waves scattering field from a rigid cylinder with a non-uniform elastic coating and immersing in an ideal fluid. Shi et al. [14] in 2018 investigated the wave scattering from an elastic sphere immersing in the water and placed in a rigid cylindrical space with an infinite length.

Inspection of multi-layered and small-sized parts like copper-clad steel rods is a hard and complex task. One of the inspection methods for these parts is using the ultrasonic waves scattered from bodies. The form function is one of the important data available in the scattering response of bodies under the radiation of the ultrasonic waves. Correct calculation of the form function is valuable due to the worthwhile information that this function contains. Because using this diagram, the inspection of the part under ultrasonic waves exposure is provided. The finite element method (FEM) is used as one of the solvers for complex engineering problems due to its high robustness and capability. Nowadays, the runtime of this method is decreased by technology development and the method is widely used in engineering problems. For the first time in this research, the form function of a copper-clad steel rod that is immersed in water is calculated using the FEM available in the commercial ABAQUS software. In recent years, researchers have investigated the effects of energy and surface parameters on the structure's behavior, and they have observed the significant effect of these factors on mechanical behavior of structure [15]. The protective clad corrosion and interfacial disbond between the rod and clad are the two most common defects of the steel rods with the copper-clad. For this reason, the effects of the location of the interfacial disbond between the rod and clad, and its arc length, and also the effects of the location and percentage of the clad corrosion on the field of the backscattered ultrasonic wave are studied in this research.

2. Ultrasonic Resonance Spectrum Theory

When the wave impacts the interface of two bodies with different mechanical properties, phenomena such as refraction, reflection, and mode conversion may occur. If the interface of two bodies is curved, not necessarily circular, the scattering phenomenon occurs under a special condition. According to the frequency spectrum resonance scattering theory, besides the smooth background, the backscattering from the elastic body contains valleys and peaks that coincide with the resonance frequencies of the body. The information embedded in the frequency spectrum of the scattered wave is studied using the ultrasonic resonance spectrum theory. In this method, a broadband ultrasonic wave is radiated to the body. At the moment of the sound wave impact on the interface of two bodies, surface waves are formed around it. If even one of the natural frequencies of the reflecting body were present in the incident wave frequency domain, these waves would have constructive interference leading to the standing wave formation. In this case, the body acts as a wave generator source that radiates energy to the surrounding.

In this paper, the experimental condition for the scattering of the ultrasonic waves from a copper-clad steel cylinder that is immersing in water is simulated using the FEM. The experimental study and evaluation of the resonance spectrum are possible using the quasi-harmonic and short-pulse method. The single frequency wave is used in the quasi-harmonic method. While a broadband short-pulse wave is sent to the objective is used in the short-pulse method. Due to the less runtime of the short-pulse method, it is used in this paper. In this method, the elastic body goes under a short-pulse incident wave with a wide frequency bandwidth. Based on this condition, the transfer function of the measurement system influences the received frequency spectrum and the frequency spectrum of the scattered wave is a combination of the one from the transducer, measurement system, and that from the backscattering waves produced by the elastic body. The resonance frequencies of the elastic body are identified by removing the measurement system frequency spectrum from that of the backscattering.

The frequency spectrum of the reflecting echo [6] is used as the reference spectrum in the modified short pulse Method of Identification and Isolation of Resonances (MIIR) technique instead of the reflected spectrum from a rigid and low diameter cylinder [16]. The form function is obtained by omitting the frequency spectrum of the measurement system from that of the received signal and drawing the obtained spectrum with respect to the normalized frequency Ka , where $K = w/c$ is the wave number, w is the angular frequency, c is the wave speed in the water environment and a is the cylinder radius. The equation for calculating the form function of the elastic cylinder is given by Eq. (1) [6]:

$$|f_{\infty}| = \left| \frac{S_{(w)}}{S'_{(w)}} \right| \left| \frac{-2}{\sqrt{\pi i K a}} \sum_{n=0}^{\infty} \frac{J'_n(Ka)}{H^{(1)'}_n(Ka)} \cos(n\varphi) \right| \quad (1)$$

in which $S_{(w)}$ is the frequency spectrum of the received signal, $S'_{(w)}$ the reflection wave frequency spectrum, φ the receiving angle, J_n the Bessel function, H_n the Henkel function and ε_n the Neumann function. The Neumann function relation is given by Eq. (2).

$$\varepsilon_n = \begin{cases} 1 & \text{for } n = 0 \\ 2 & \text{for } n \geq 1 \end{cases} \quad (2)$$

3. FEM Simulation

In the FEM, the problems are analyzed based on dividing the body into smaller parts, each part is called an "element". In other words, by putting the results of elements together in FEM, the response of the governing equations of the problem is obtained. Nowadays, the runtime of this method is decreased by technology development and the method is widely used in engineering problems, including wave propagation. The explicit and implicit methods provide solving the FE equations. The explicit method is used in this paper for investigating the scattering phenomenon due to the dynamic basis of the wave propagation, small-time steps, and a high number of nodes.

The studied part is a copper-clad steel cylinder with an infinite length and circular cross-section which is immersed in the water. Force, pressure, or displacement exertions are some methods for modeling the piezoelectric effect, the wave generation, in the FEM. In this research, the pressure exertion method is used for modeling the piezoelectric. Equation (3) is used for calculating the exerted pressure value by placing the normal transducer on the part, using the pulse form [17]:

$$\begin{aligned} & \left(1 - \cos\left(\frac{2\pi ft}{N}\right)\right) \cos(2\pi ft) \quad \text{for } 0 < t < \frac{N}{f} \\ & 0 \quad \text{otherwise} \end{aligned} \quad (3)$$



where f is the excitation frequency in Hz, N number of excitation signal cycles and t is the excitation time. The radiant wave in this research has 2 cycles, and its center frequency is 1 MHz. The time signal of the sent wave and its frequency spectrum are shown in Fig. 2 and Fig. 3, respectively.

The dimensions of the part and the way of locating the ultrasonic probe are shown in Fig. 1. The infinite length condition of the cylinder is met by selecting the four-node plane strain element (CPE4R). The existence of reflected waves from the walls in the received signal hardens the interpretation of the results. To prevent interference of the reflected waves from walls and scattering waves, the 4-node linear plane strain one-way infinite quadrilateral element (CINPE4) is used at the walls. Figure 4 shows the way of using finite and infinite elements. The water in this paper is modeled as a quasi-elastic state. The incompressibility of water is satisfied by setting the Poisson's ratio to a value of around 0.5. Furthermore, a small Young's modulus and very small shear and large bulk modulus are devoted to the water. Table 1 shows the mechanical properties of the materials. Because of using the explicit solver of the ABAQUS software, the minimum time step for making sure that the solution is convergent is obtained using the following equation:

$$\Delta t \leq \Delta t_{cr} = \frac{l_{min}}{c_l} \quad (4)$$

in which l_{min} and c_l are the smallest sizes of the element and longitudinal wave speed in the body, respectively. To use a good shape function for accurate calculation of related parameters, and preventing the solution divergence, the size of the element is determined based on the smallest wavelength, λ_{min} , given by Eq. (5) [18]:

$$l_{min} \leq \frac{\lambda_{min}}{20} \quad (5)$$

In this research, the size of the element is 21, 84, and 64 micrometers for the water, steel, and copper-clad, respectively.

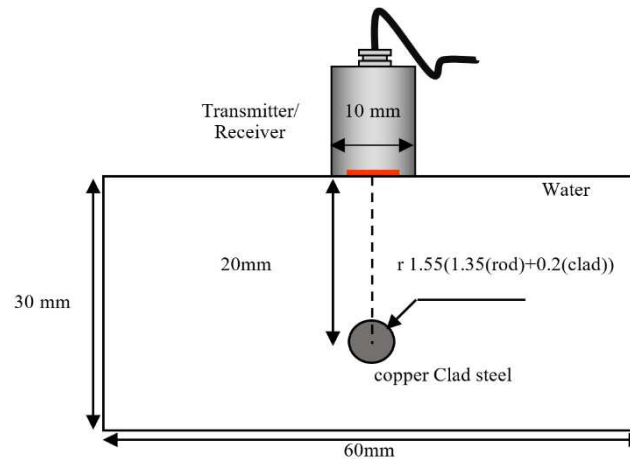


Fig. 1. Schematic of the coated cylinder geometrical structure embedded in the water.

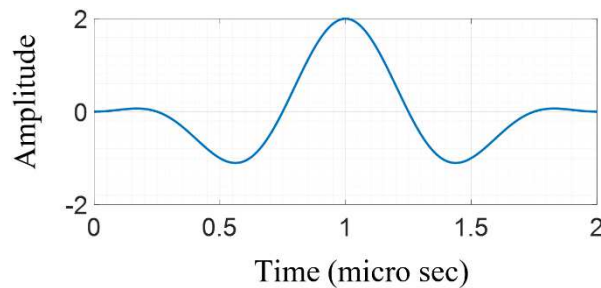


Fig. 2. The radiant wave with the frequency of 1MHz and cycle number of $N = 2$.

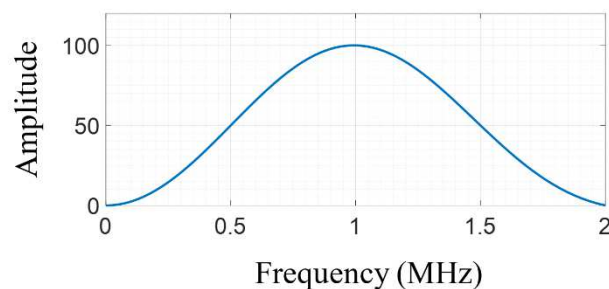


Fig. 3. The frequency spectrum of the radiant wave.



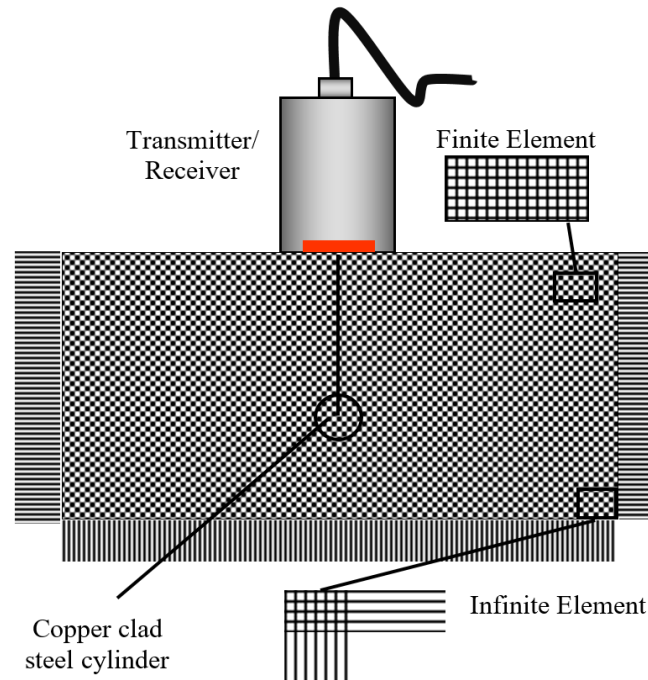
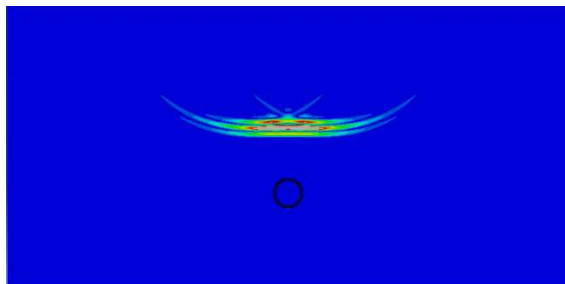
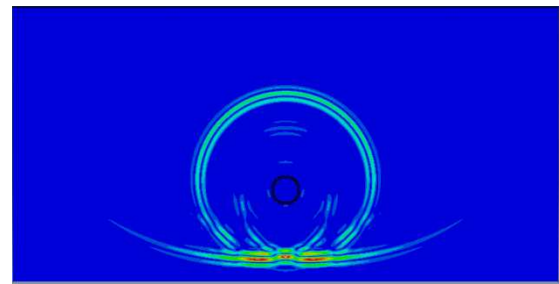
Table 1. The mechanical properties and elastic constants of materials.

Material	Density (Kg/m ³)	Young module (Pa)	Poisson ratio
Steel	7800	208e9	28·0
Water	1000	2999.99954346217	0.499999771731086
Copper	8940	110e9	33·0

4. Numerical Results

4.1 Validation

The accuracy of the numerical model is evaluated by comparing the form function of the copper-clad steel cylinder obtained from the FEM with those from analytical and experimental [19] results. The form function is calculated using a normal transmitter-receiver probe on the copper-clad steel cylinder immersed in the water. Figure 2 and Fig. 3 show the sent pulse and its equivalence in the frequency field. The sent pulse has a central frequency of 1MHz and bandwidth of 0.5-1.5MHz. Therefore, the results are valid in the normalized frequency, Ka , range of 3 to 10. Figure 5 shows the way of ultrasonic wave propagation in water, and Fig. 6 shows the scattering of the wave after impinging on the copper-clad steel cylinder. The received signal and its corresponding reflecting echo are shown in Fig. 7. Furthermore, the frequency spectrum of the backscattered signal and received reflection echo are depicted in Fig. 8. The form function of the cylinder is calculated using the information given by Fig. 8 in Eq. (1). The resonance frequencies are represented using the (n,l) index, where n indicates the wavenumber, which is half of the nodes number around the cylinder at the constant frequency and standing wave state, and l represents the wave kind around the cylinder. $l = 1$ represents the pseudo-Rayleigh waves, and $l = 2, 3, \dots$ represents the whispering gallery waves. The proposed model is validated by comparing this form function with those calculated using the analytical and experimental methods (see Fig. 9). As observed, an excellent agreement is observed between the results in terms of the overall form of the form function and the location of the resonance frequencies. Furthermore, the values of the normalized frequencies in the results of current research are compared with those of the previous experimental works in Table 2.

**Fig. 4.** The locating structure of the elements in FEM.**Fig. 5.** Propagation of the ultrasonic waves in water.**Fig. 6.** Scattering of the ultrasonic waves after impacting the copper-clad steel rod is immersed in water.

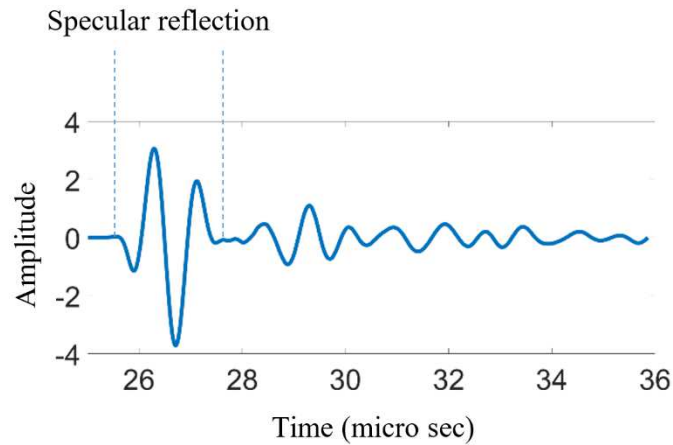


Fig. 7. The backscattering time signal from the copper-clad steel cylinder is immersed in water.

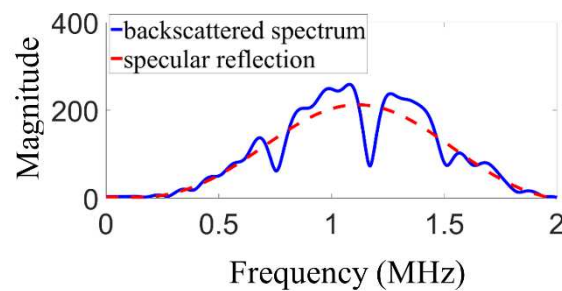


Fig. 8. The frequency spectrum of the backscattering time signal and reflection echo from the copper-clad steel cylinder immersed in water.

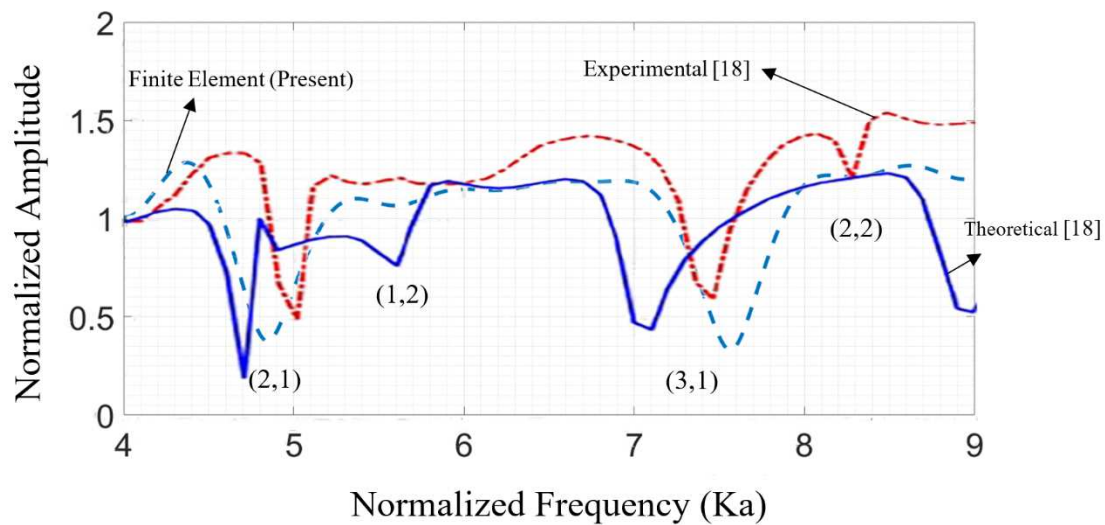


Fig. 9. The form function of the copper-clad steel cylinder immersed in water using the FEM, analytical and experimental [19] methods.

4.2. Interfacial disbond defect between the clad and cylinder

In this section, the effects of the interfacial disbond defect between the clad and cylinder on the backscattering wave field is evaluated. In finite element model, the disbond effect zone between two surfaces has no constraint. However, the remaining surfaces with full bond between two objects are connected by tie constraint. The received signal and presence of this defect are analyzed using the modified short pulse MIIR technique. The effects of the length and location of this defect on the far-field backscattered frequency spectrum is investigated.

Table 2. Value of the normalized resonance frequency of the form function of the copper-clad steel cylinder immersed in water using the FEM and experimental [19] methods.

Mode number (n,l)	(2,1)	(1,2)	(3,1)	(2,2)
Resonance frequency (Ka) using experimental method [18]	5.01	5.83	7.47	8.28
Resonance frequency (Ka) using finite element method(present)	4.9784	6.0345	7.6998	8.5464



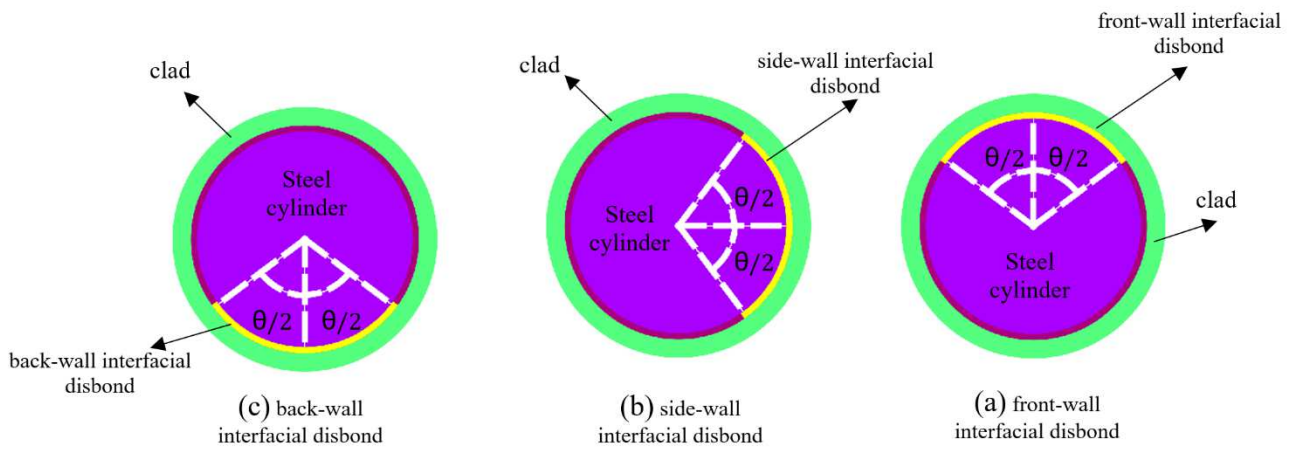


Fig. 10. Schematic and position of the interfacial disbond between the steel cylinder and copper-clad.

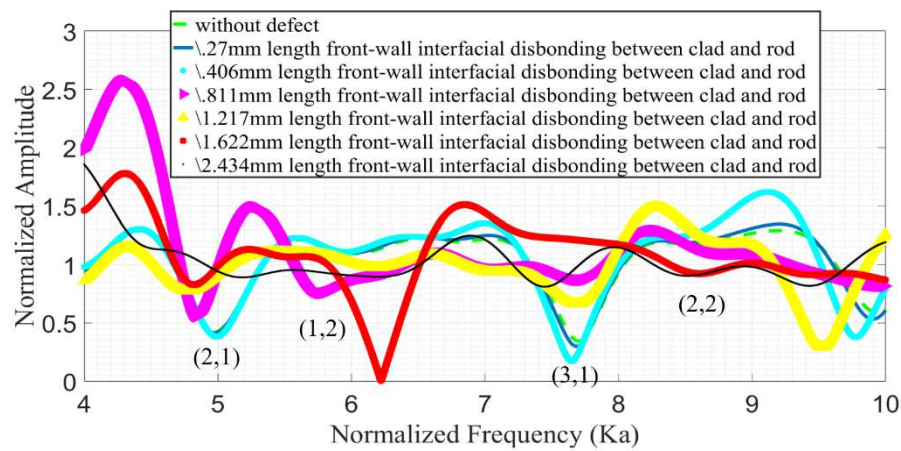


Fig. 11. The form function of the copper-clad steel rod immersing in water using the FEM in the intactness and existence of the front-wall interfacial disbond defect.

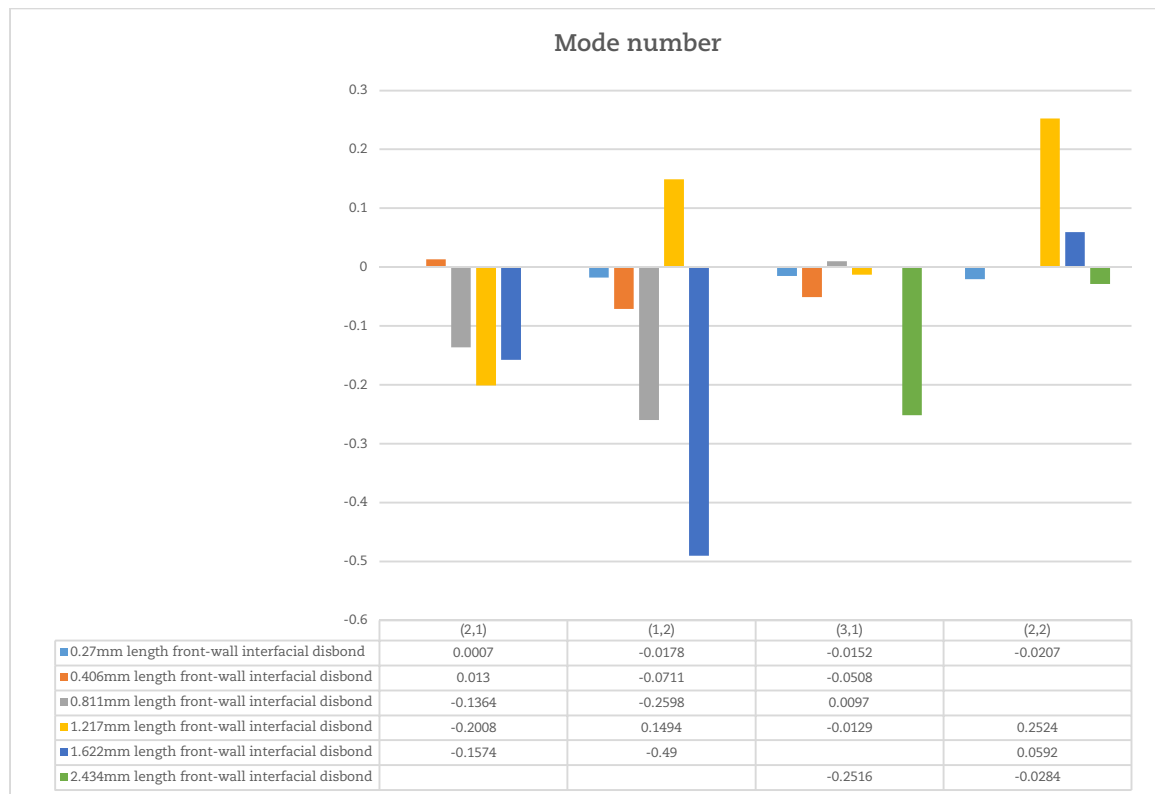


Fig. 12. Variation of the normalized resonance frequency due to the existence of the front-wall interfacial disbond defect.



Table 3. Value of the normalized resonance frequency due to the existence of the front-wall interfacial disbond defect.

Mode number (n,l)	(2,1)	(1,2)	(3,1)	(2,2)
Resonance frequency (ka) without defect	4.9784	6.0345	7.6998	8.5464
Resonance frequency (ka) when there is a .27mm length front-wall between cladding and rod	4.9791	6.0167	7.6846	8.5257
Resonance frequency (ka) when there is a .406mm length front-wall between cladding and rod	4.9914	5.9574	7.6490	Not detect
Resonance frequency (ka) when there is a .811mm length front-wall between cladding and rod	4.8420	5.7747	7.7095	Not detect
Resonance frequency (ka) when there is a 1.217mm length front-wall between cladding and rod	4.7776	6.1839	7.6869	8.7988
Resonance frequency (ka) when there is a 1.622mm length front-wall between cladding and rod	4.8210	5.5445	Not detect	8.6056
Resonance frequency (ka) when there is a 2.434mm length front-wall between cladding and rod	Not detect	Not detect	7.4482	8.5180

4.2.1 Front-wall interfacial disbond defect

In this section, the front-wall interfacial disbond defect and the effects of its arc length on the form function are studied. The schematic of these defects' positions is shown in Fig. 10a. The effects of the arc length of this defect on the wave field is evaluated. After analysis of the received signal and using the short pulse MIIR technique, the form function in the presence of this defect is drawn and compared with the form function of the intact coated cylinder (Fig. 11). Figure 12 shows the variation of the normalized frequencies with different arc lengths of this defect. Table 3 shows the accurate value of these normalized frequencies as the arc length is increased. The location of the (2,1) frequency mode in this defect for the defect length below 0.811mm is not considerably changed compared to the one for the intact coated steel cylinder. However, the location of this mode is decreased sharply with an increase of the defect length up to the 0.811mm value. Further increase of the length above this value leads to no considerable change in the location of this mode and finally, this mode cannot be specified as the defect length reaches its maximum value. Value of the (1,2) frequency mode has a descending trend as the length of the defect is increased up to 0.811mm. At this value, the location of this mode is increased sharply and is decreased again after that. The location of the (3,1) normalized frequency mode is not changed considerably as the defect length is increased up to 1.622mm, at which specifying the amount of this mode is not possible. With a further increment of the defect length of this mode and reaching its maximum value, this mode is specified again but its value is sharply decreased. Furthermore, the (2,2) mode cannot be specified as the defect length is increased up to 0.406mm. After 0.406mm, the value of this mode is increased sharply up to 1.217mm after which the mode value is decreased again.

4.2.2 Side-wall interfacial disbonding defect

The side-wall interfacial disbond defect and the effects of its arc length on the received signal are studied in this section. The schematic of these defects' positions is shown in Fig. 10b. The effects of the arc length of this defect on the location of the normalized frequencies of the form function is evaluated.

The received signal is processed using the short pulse MIIR technique and then the form function of these models is drawn. The form function in the presence of these defects is compared with the one corresponding to the intact coated cylinder in Fig. 13. Figure 14 shows the variation of the normalized frequencies with the arc length of this defect relative to the intact state. The accurate values of these normalized frequencies are calculated in Table 4.

Location of the (2,1) frequency mode is first decreased as the defect length increases but is considerably increased at the defect length of 0.811mm. Above this value, the location of this mode is again decreased by the defect length increase. The (1,2) mode is first decreased a little but is highly increased when the defect length reaches 0.811mm. This mode is increased with the further increase of the defect length above 0.811mm. The (3,1) mode is also decreased a little with the defect length up to 0.811mm at which it is increased. This mode is decreased with the further increase of the defect length, but at the maximum defect length of 2.434, the value of this mode is increased sharply. The (3,1) frequency mode is not changed considerably as the defect length is increased up to 0.811mm, at which this mode cannot be specified anymore.

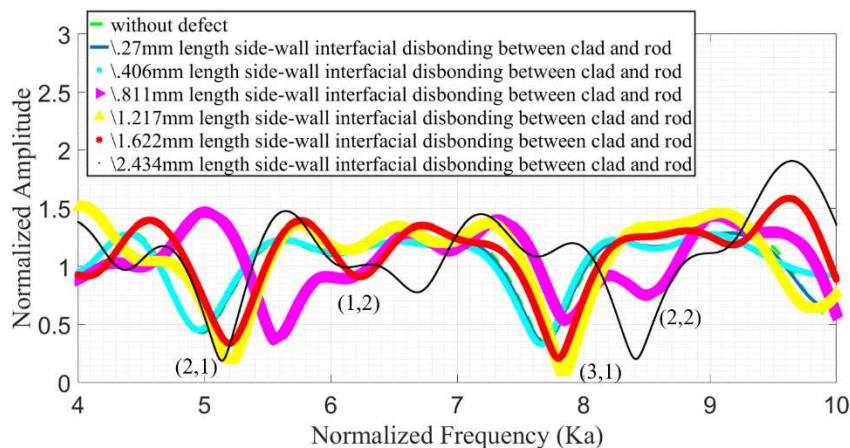
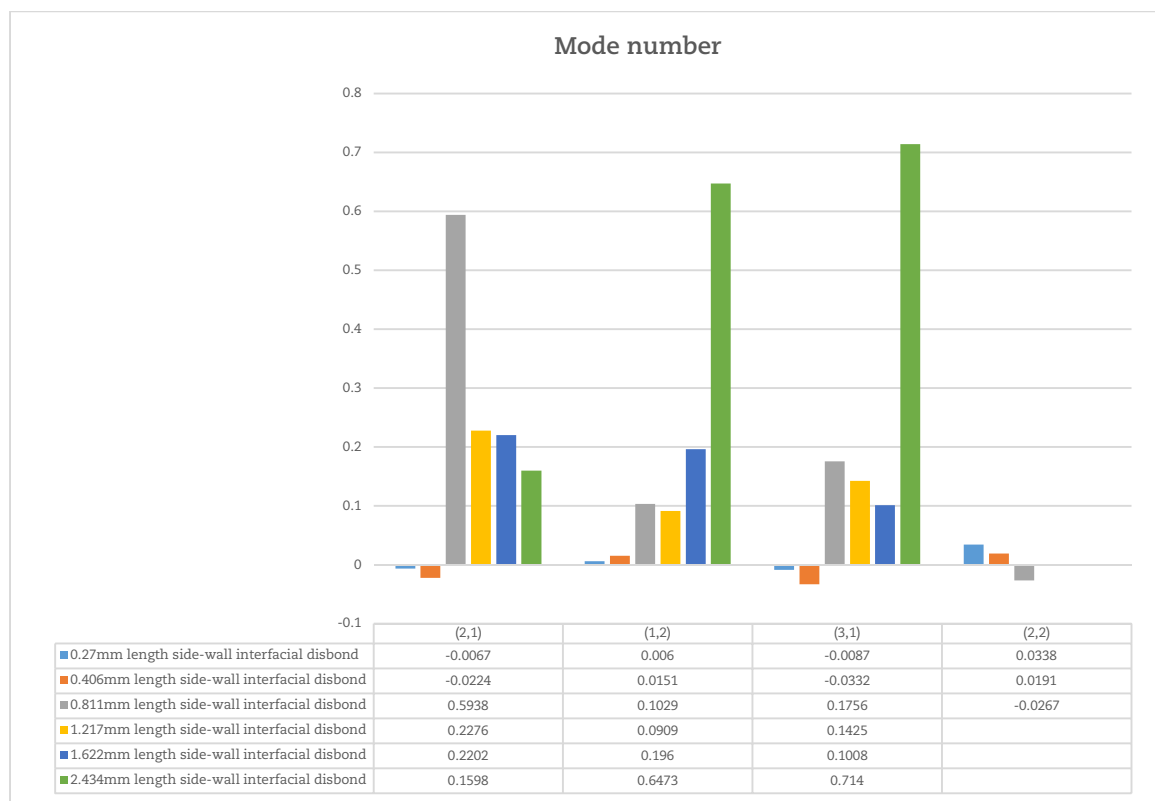


Fig. 13. The form function of the copper-clad steel rod immersing in water using the FEM in case of the intact cylinder and existence of the side-wall interfacial disbond defect.



Table 4. Value of the normalized resonance frequency due to the existence of the side-wall interfacial disbond defect.

Mode number (n,l)	(2,1)	(1,2)	(3,1)	(2,2)
Resonance frequency (ka) without defect	4.9784	6.0345	7.6998	8.5464
Resonance frequency (ka) when there is a .27mm length side-wall disbond between cladding and rod	4.9717	6.0405	7.6911	8.5802
Resonance frequency (ka) when there is a .406mm length side-wall disbond between cladding and rod	4.9560	6.0496	7.6666	8.5655
Resonance frequency (ka) when there is a .811mm length side-wall disbond between cladding and rod	5.5722	6.1374	7.8754	8.5197
Resonance frequency (ka) when there is a 1.217mm length side-wall disbond between cladding and rod	5.2060	6.1254	7.8423	Not detect
Resonance frequency (ka) when there is a 1.622mm length side-wall disbond between cladding and rod	5.1986	6.2305	7.8006	Not detect
Resonance frequency (ka) when there is a 2.434mm length side-wall disbond between cladding and rod	5.1382	6.6818	8.4138	Not detect

**Fig. 14.** Variation of the normalized resonance frequency due to the existence of the side-wall interfacial disbond defect.

4.2.3. Back-wall interfacial disbonding defect

In this section, the effects of the interfacial disbond defect at the back-wall of the cylinder and also the effects of its arc length on the form function are studied. The schematic and position of these defects are shown in Fig. 10c. Furthermore, the effects of the arc length of this defect on the values of the normalized frequencies of the form function is evaluated. Like the previous models, the received signal of these models is also studied and their form function is plotted. The form function in the presence of these defects is compared with the one corresponding to the intact coated cylinder in Fig. 15. Furthermore, figure 16 shows the variation of the non-dimensional frequencies with the arc length of this defect, relative to the intact cylinder state. The accurate values of these normalized frequencies are presented in Table 5. As observed in Table 5 and Fig. 16, the location of the (2,1) frequency mode is increased sharply up to the defect length of 0.811mm and is decreased after that. The (1,2) mode is first decreased but is sharply increased when the defect length reaches 0.811mm. Then this mode is decreased again with the further increase of the defect length up to 1.217mm, reaching the same value as its initial one, corresponding to the intact condition of this mode. Value of the (3,1) frequency mode has an ascending trend as the length of the defect is increased up to 0.811mm and is decreased after that. The maximum jump in this mode occurs when the defect length reaches its maximum value. The location of the (2,2) frequency mode is not changed considerably in the presence of this defect regardless of its arc length amount. Only when the defect length reaches its maximum value, the location of this mode cannot be determined anymore.



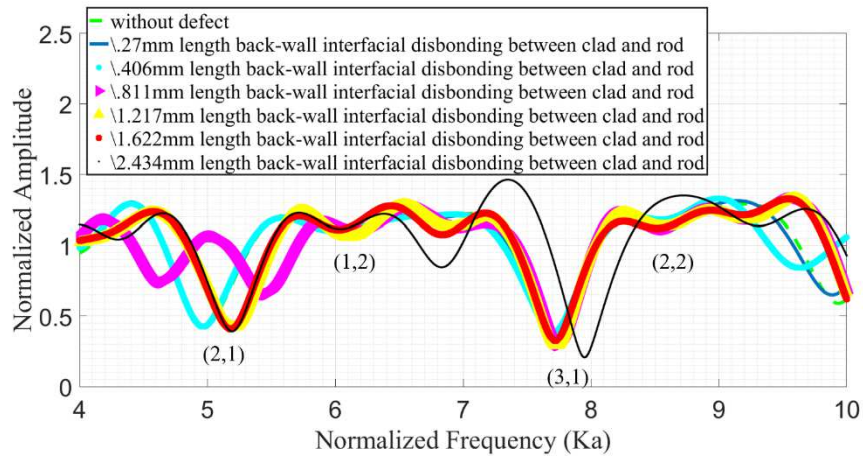


Fig. 15. The form function of the copper-clad steel rod immersing in water using the FEM in case of the intact rod and existence of the back-wall interfacial disbond.

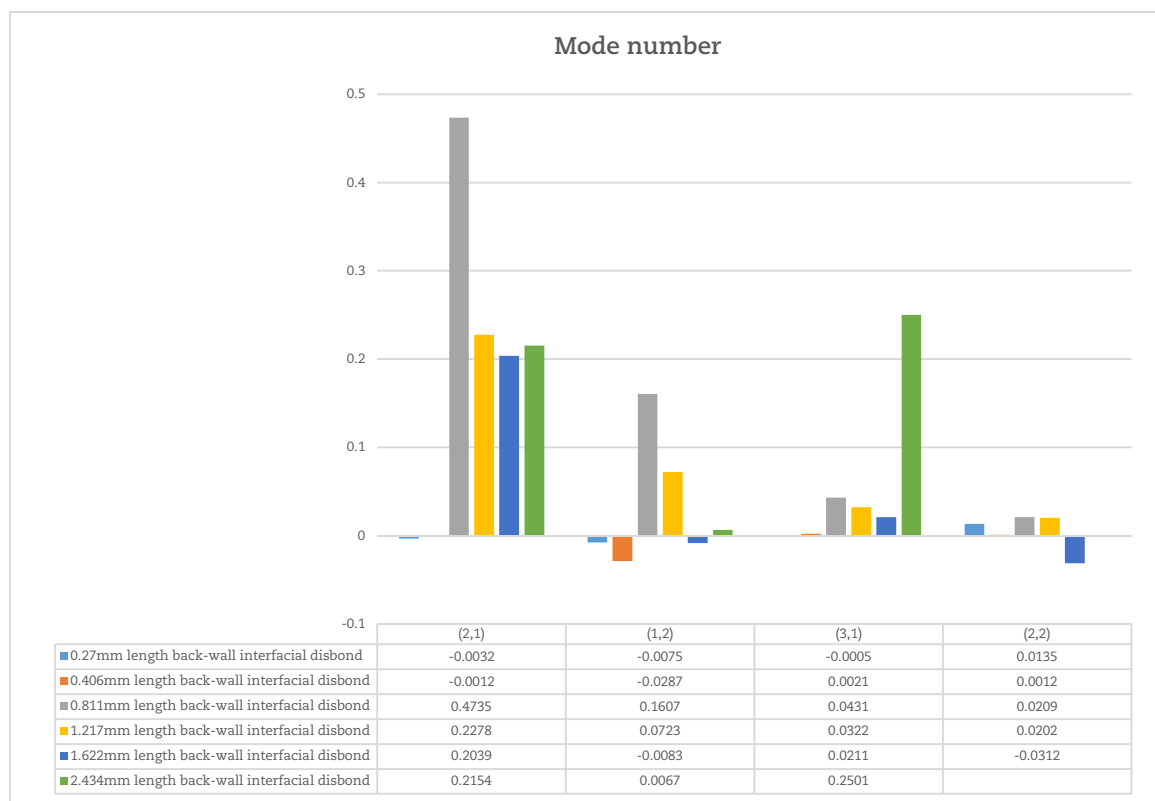


Fig. 16. Variation of the normalized resonance frequency due to the existence of the back-wall interfacial disbond.

Table 5. Value of the normalized resonance frequency due to the existence of the back-wall disbond.

Mode number (n,l)	(2,1)	(1,2)	(3,1)	(2,2)
Resonance frequency (ka) without defect	4.9784	6.0345	7.6998	8.5464
Resonance frequency (ka) when there is a .27mm length back-wall disbond between cladding and rod	4.9752	6.0270	7.6993	8.5599
Resonance frequency (ka) when there is a .406mm length back-wall disbond between cladding and rod	4.9664	6.0058	7.7019	8.5476
Resonance frequency (ka) when there is a .811mm length back-wall disbond between cladding and rod	5.4519	6.1952	7.7429	8.5673
Resonance frequency (ka) when there is a 1.217mm length back-wall disbond between cladding and rod	5.2062	6.1068	7.7320	8.5666
Resonance frequency (ka) when there is a 1.622mm length back-wall disbond between cladding and rod	5.1823	6.0262	7.7209	8.5152
Resonance frequency (ka) when there is a 2.434mm length back-wall disbond between cladding and rod	5.1938	6.0412	7.9499	Not detect



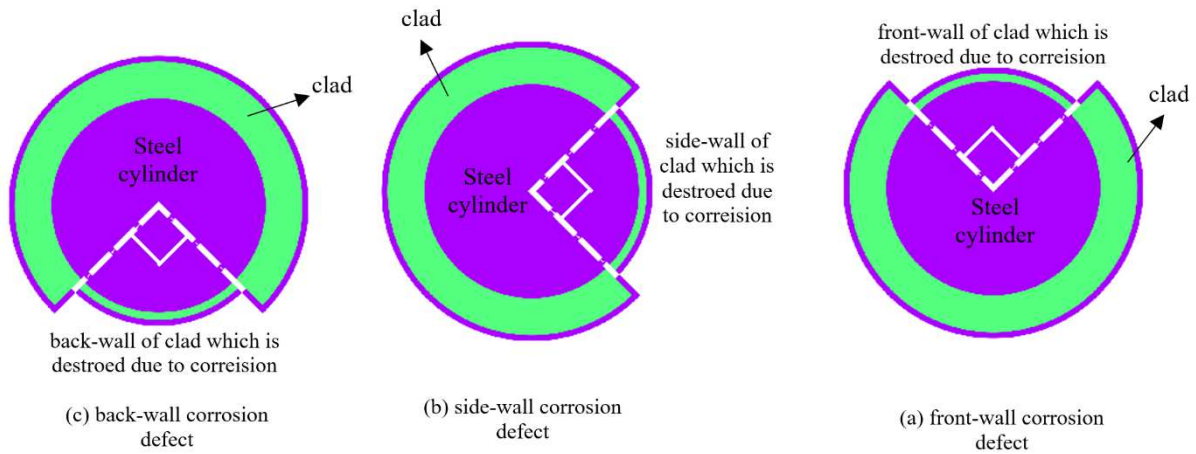


Fig. 17. Schematic and position of the Corrosion defect in the cylinder clad

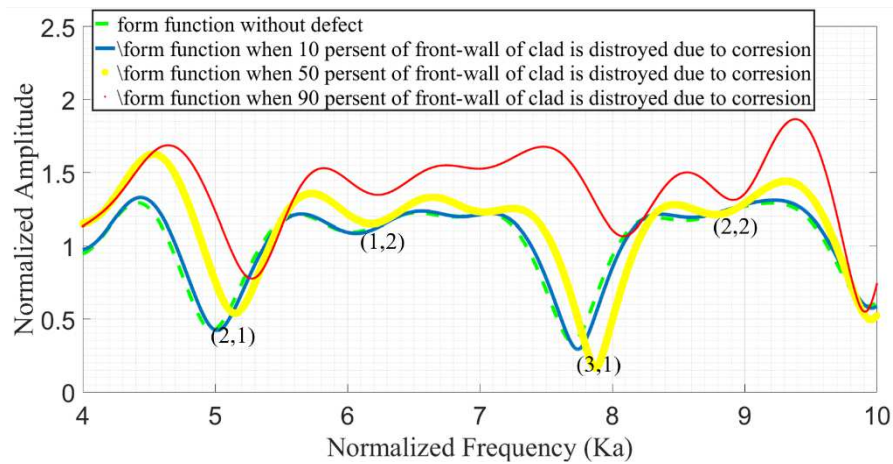


Fig. 18. The form function of the copper-clad steel rod immersing in water using the FEM in case of the intact cylinder and existence of the front-wall corrosion defect.

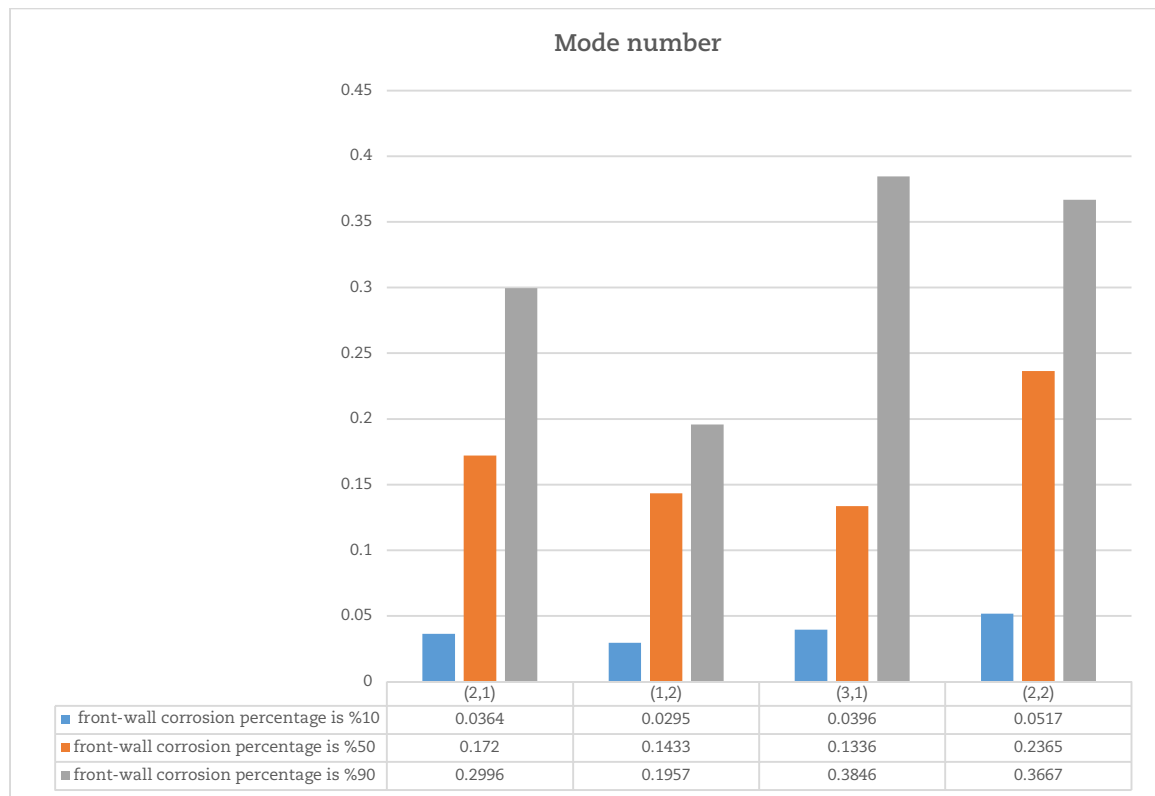


Fig. 19. Variation of the normalized resonance frequency due to the existence of the front-wall corrosion defect.

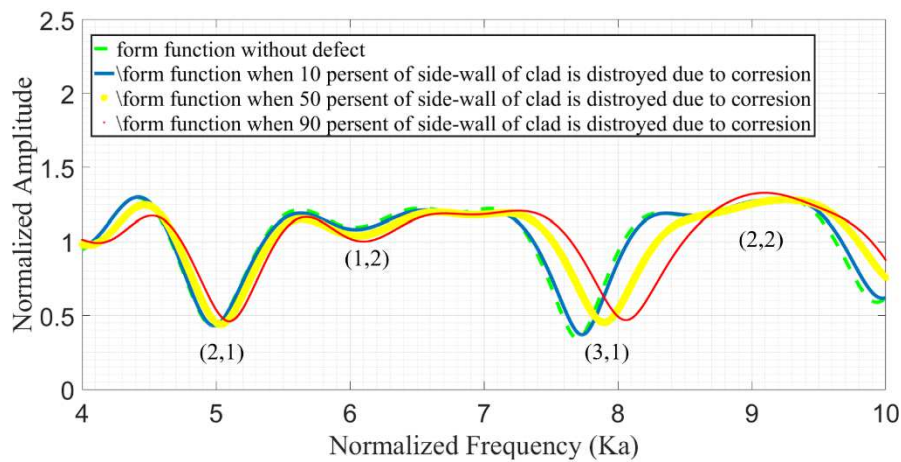
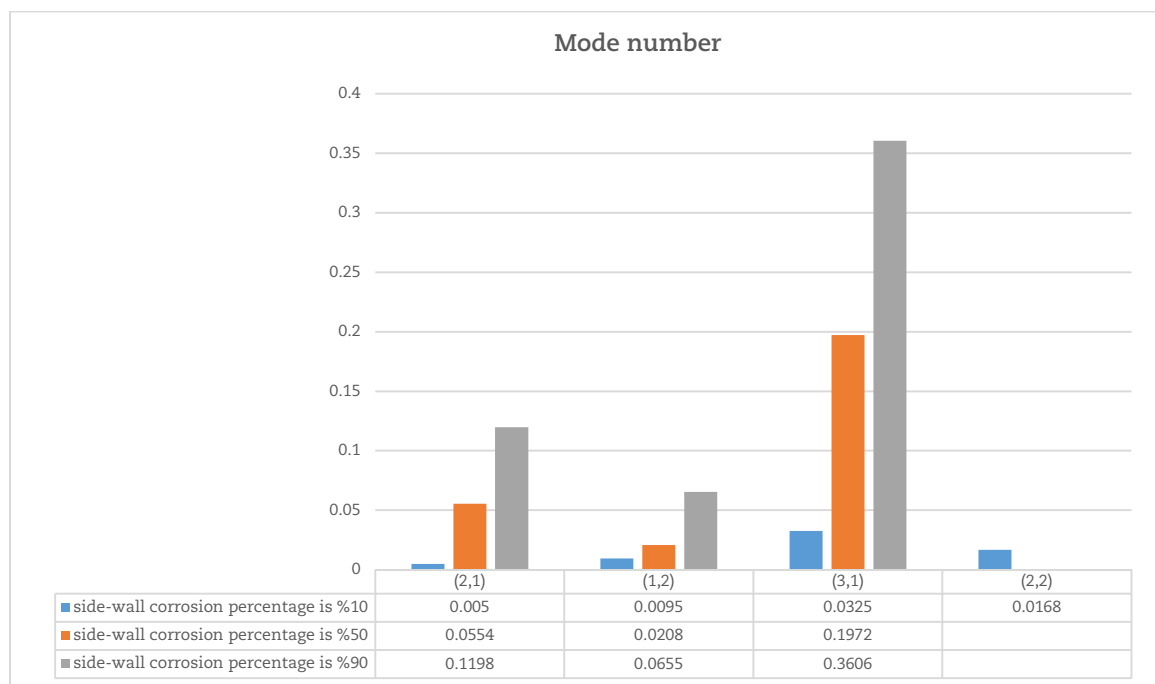


Table 6. Value of the normalized resonance frequency due to the existence of the side-wall corrosion defect.

Mode number (n,l)	(2,1)	(1,2)	(3,1)	(2,2)
Resonance frequency (ka) when there is no defect in the rod	4.9784	6.0345	7.6998	8.5464
Resonance frequency (ka) when 10 percent of front-wall cladsrod is destroyed due to corrosion	5.0148	6.0640	7.7394	8.5981
Resonance frequency (ka) when 50 percent of front-wall cladsrod is destroyed due to corrosion	5.1504	6.1778	7.8730	8.7829
Resonance frequency (ka) when 90 percent of front-wall cladsrod is destroyed due to corrosion	5.2780	6.2302	8.0844	8.9131

Table 7. Value of the normalized resonance frequency due to the existence of the side-wall corrosion defect.

Mode number (n,l)	(2,1)	(1,2)	(3,1)	(2,2)
Resonance frequency (ka) when there is no defect in the rod	4.9784	6.0345	7.6998	8.5464
Resonance frequency (ka) when 10 percent of side-wall cladsrod is destroyed due to corrosion	4.9834	6.0440	7.7323	8.5632
Resonance frequency (ka) when 50 percent of front side-wall cladsrod is destroyed due to corrosion	5.0338	6.0553	7.8970	Not detect
Resonance frequency (ka) when 90 percent of front side-wall cladsrod is destroyed due to corrosion	5.0982	6.1000	8.0604	Not detect

**Fig. 20.** The form function of the copper-clad steel rod immersing in water using the FEM in case of the intact cylinder and the existence of the side-wall corrosion defect.**Fig. 21.** Variation of the non-dimensional resonance frequency due to the existence of the side-wall corrosion defect.

4.3. Corrosion defect in the cylinder clad

The corrosion defect is of the most common defects of the coated cylinders. In this research, the effects of the clad corrosion on the backscattered ultrasonic wave is studied. For this purpose, the effects of the corrosion percentage and location on the results obtained from the wave field are investigated.

4.3.1. Front-wall corrosion defect

The schematic and position of this defect are shown in Fig. 17a. In this section, the effects of the corrosion percentage, at the front-wall, on the wave behavior is evaluated. Using the deconvolution of the received signal, the form function of these models is also drawn. The form function of these models is drawn in Fig. 18. Values of the normalized frequencies of form functions in the presence of this defect and their variation relative to the intact cylinder are presented in Table 6 and Fig. 19, respectively. Results show that amount of all frequency modes in this defect is increased with the corrosion amount.

4.3.2. Side-wall corrosion defect

Figure 17b shows the schematic and position of this defect. The goal of this model is to evaluate the behavior of the ultrasonic wave field in the presence of this defect and the effects of the corrosion percentage on the results. The form functions of these models are calculated after performing the mathematical operations and calculations on the received signal (see Fig. 20). For a better evaluation of the results, the normalized frequencies of the form functions in the presence of this defect and their variations relative to those obtained from the intact cylinder are shown in Table 7 and Fig. 21, respectively.

Location of frequency modes of (2,1), (1,2), and (3,1) is increased with the corrosion amount. Value of the (2,2) mode is increased in case the corrosion percentage is %10. With the further increase and reaching the %50 corrosion and above, it is impossible to specify the location of this mode.

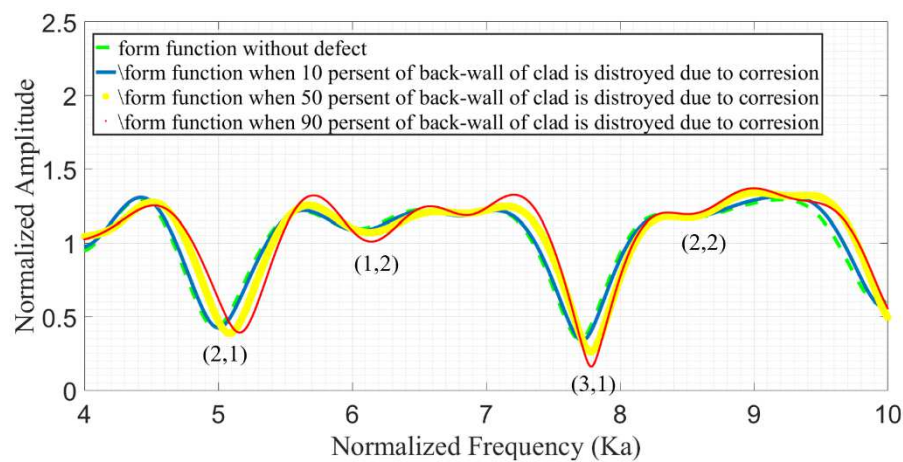


Fig. 22. The form function of the copper-clad steel rod immersing in water using the FEM in the intactness state and existence of the back-wall corrosion defect.

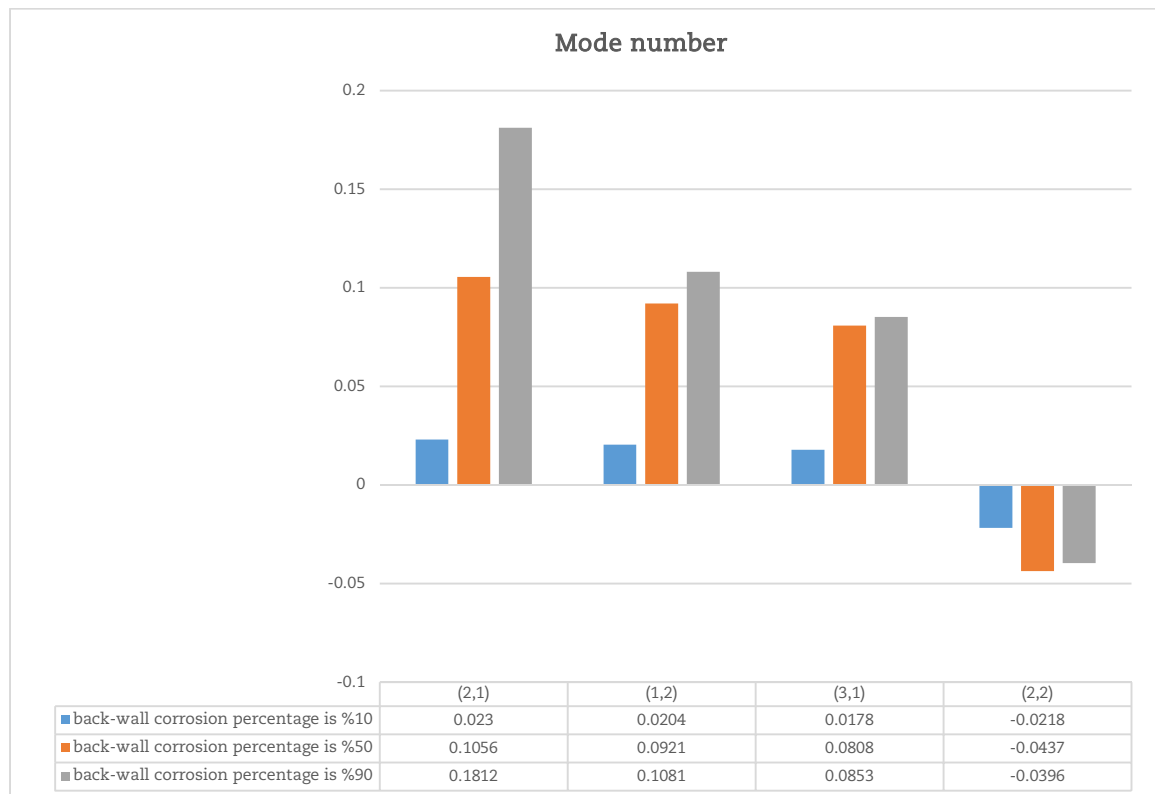


Fig. 23. Variation of the normalized resonance frequency due to the existence of the back-wall corrosion defect.



Table 8. Value of the normalized resonance frequency due to the existence of the back-wall corrosion defect.

Mode number (n,l)	(2,1)	(1,2)	(3,1)	(2,2)
Resonance frequency (ka) when there is no defect in the rod	4.9784	6.0345	7.6998	8.5464
Resonance frequency (ka) when 10 percent of back-wall cladsrod is destroyed due to corrosion	5.0014	6.0549	7.7176	8.5246
Resonance frequency (ka) when 50 percent of front back-wall cladsrod is destroyed due to corrosion	5.0840	6.1266	7.7806	8.5027
Resonance frequency (ka) when 90 percent of front back-wall cladsrod is destroyed due to corrosion	5.1596	6.1426	7.7851	8.5068

4.3.3 Corrosion defect at the cylinder back-wall

Figure 17c shows the schematic and schematic of this defect. The field of the backscattered ultrasonic wave at the situation that the defect is presented at the cylinder back-wall and the effects of the clad corrosion percentage on the form function is investigated for this state. The form function in this model is similarly calculated using the MIIR technique applied to the received signal (Fig. 22). Figure 23 and Table 8 show the obtained results from these models.

The location of (2,1), (1,2), and (3,1) frequency modes is increased as the corrosion amount is increased. However, the (2,2) frequency mode has different behavior and is decreased as the corrosion amount is increased such that the possibility of specifying the location of this mode is eventually canceled as the corrosion amount reaches %90.

5. Conclusions

Correct calculation of the scattering field is crucial for using ultrasonic waves. The form function is an obtained result from the scattering field. The precise calculating of this diagram is very important because the intactness of the body can be studied using that. For the first time in this research, the form function of a copper-clad steel rod that is immersed in water is calculated using the FEM available in the commercial ABAQUS software. The precision and correctness of the proposed model are evaluated by comparing the results with those from analytical and experimental. The value of resonance frequencies and the obtained form function have good agreements with the analytical and experimental results that manifest the correctness of the proposed model. Furthermore, the possibility of using the backscattered frequency spectrum for specifying two common defects in these rods, i.e., the corrosion of the rod coating and separation of the coating from the steel rod, was investigated. It was found that the location of the corrosion and interfacial disbond between the clad and rod defect, the corrosion amount, and the length of the interfacial disbond defect can be specified using the backscattering ultrasonic waves.

Author Contributions

O. Noormohammadi Arani started research and expand finite element model and examined the model validation. Manuscript was written by O. Noormohammadi Arani and M. Zeighami Salimabad. All authors discussed the results, reviewed, and approved the final version of the manuscript.

Acknowledgments

Not applicable.

Conflict of Interest

The authors declared no potential conflicts of interest with respect to the research, authorship, and publication of this article.

Funding

The authors received no financial support for the research, authorship, and publication of this article.

Data Availability Statements

The datasets generated and/or analyzed during the current study are available from the corresponding author on reasonable request.

References

- [1] Yilmaz, B., Jasiūnienė, E., Advanced ultrasonic NDT for weak bond detection in composite-adhesive bonded structures, *International Journal of Adhesion and Adhesives*, 102, 2020, 102675.
- [2] Jain, H., Tarpara, E.G., Patankar, V.H., Design and development of ultrasonic bipolar square-wave pulser for non-destructive testing of concrete structures, *Review of Scientific Instruments*, 91(9), 2020, 094704.
- [3] Qina, F., Wu, Y., Guo, H., Zheng, B., Liu, H., Laser Ultrasonic Nondestructive Testing Based on Nonlinear Ultrasonic Coefficient, *Russian Journal of Nondestructive Testing*, 56(3), 2020, 209-221.
- [4] Honarvar, F., Varvani-Farahani, A., A review of ultrasonic testing applications in additive manufacturing: Defect evaluation, material characterization, and process control, *Ultrasonics*, 108, 2020, 106227.
- [5] Honarvar, F., Enjilela, E., *Resonance acoustic spectroscopy, Handbook of Applied Solid State Spectroscopy*, Springer, Boston, MA, 2006.
- [6] James, J., Faran, Jr., Sound scattering by solid cylinders and spheres, *The Journal of the Acoustical Society of America*, 23(4), 1951, 405-418.
- [7] Flax, L., Dragonette, L.R., Überall, H., Theory of elastic resonance excitation by sound scattering, *The Journal of the Acoustical Society of America*, 63(3), 1978, 723-731.
- [8] Shir Guran A., Guicking, D., *Acoustic Interactions with Submerged Elastic Structures*, World Scientific Publishing Co Pte Ltd, Singapore, 2001.
- [9] Honarvar, F., Sinclair, A.N., Acoustic wave scattering from transversely isotropic cylinders, *The Journal of the Acoustical Society of America*, 100(1), 1996, 57-63.
- [10] Jean, R., Maze, G., Izicki, J.-L., A new acoustic spectroscopy: Resonance spectroscopy by the MIIR, *Journal of Nondestructive Evaluation*, 5(2), 1985, 69-79.




- [11] Sodagar, S., Honarvar, F., Yaghootian, A., Sinclair, A.N., An alternative approach for measuring the scattered acoustic pressure field of immersed single and multiple cylinders, *Acoustical Physics*, 57(3), 2011, 411-419.
- [12] Jamali, J., Naei, M.H., Honarvar, F., Rajabi, M., Acoustic scattering and radiation force function experienced by functionally graded cylindrical shells, *Journal of Mechanics*, 27(2), 2011, 227-243.
- [13] Romanov, A.G., Tolokonnikov, L.A., The scattering of acoustic waves by a cylinder with a non-uniform elastic coating, *Journal of Applied Mathematics and Mechanics*, 75(5), 2011, 595-600.
- [14] Shi, J., Zhang, X., Chen, R., Zhang, G., Acoustic radiation force of a solid elastic sphere immersed in a cylindrical cavity filled with ideal fluid, *Wave Motion*, 80, 2018, 37-46.
- [15] Zhu, C.-S., Fang, X.-Q., Liu, J.-X., Li, H.-Y., Surface energy effect on nonlinear free vibration behavior of orthotropic piezoelectric cylindrical nano-shells, *European Journal of Mechanics-A/Solids*, 66, 2017, 423-432.
- [16] Li, T., Mitsuhiro, U., Sound scattering of a plane wave obliquely incident on a cylinder, *The Journal of the Acoustical Society of America*, 86(6), 1989, 2363-2368.
- [17] Noormohammadi Arani, O., Yaghootian, A., Sodagar, S., Investigation on the Crack Effect in the Cylinder and Matrix on the Backscattering Field Frequency Specifications using the Finite Element Method, *Journal of Applied and Computational Mechanics*, 2020, doi: 10.22055/JACM.2020.31700.1910.
- [18] Alleyne, D., Cawley, P., A two-dimensional Fourier transform method for the measurement of propagating multimode signals, *The Journal of the Acoustical Society of America*, 89(3), 1991, 1159-1168.
- [19] Fathi-Haftshejani, P., Honarvar, F., Nondestructive Evaluation of Clad Rods by Inversion of Acoustic Scattering Data, *Journal of Nondestructive Evaluation*, 38, 2019, 1-9.

ORCID iD

Omid Noormohammadi Arani  <https://orcid.org/0000-0002-7296-7099>

Mehdi Zeighami Salimabad  <https://orcid.org/0000-0002-6529-6004>

Amin Yaghootian  <https://orcid.org/0000-0003-0416-2202>

Mohammadreza Kari  <https://orcid.org/0000-0001-5951-491X>



© 2021 Shahid Chamran University of Ahvaz, Ahvaz, Iran. This article is an open access article distributed under the terms and conditions of the Creative Commons Attribution-NonCommercial 4.0 International (CC BY-NC 4.0 license) (<http://creativecommons.org/licenses/by-nc/4.0/>).

How to cite this article: Noormohammadi Arani O., Salimabad M.Z., Yaghootian A., Kari M. Calculation of Backscattered Ultrasonic Waves Field from a Copper-clad Steel Rod Immersing in Water and Effect of Clad Corrosion and Interfacial Disbond between Clad and Rod Defects on this Field using the Finite Element Method, *J. Appl. Comput. Mech.*, 9(1), 2023, 58-71. <https://doi.org/10.22055/JACM.2021.38098.3172>

Publisher's Note Shahid Chamran University of Ahvaz remains neutral with regard to jurisdictional claims in published maps and institutional affiliations.

